16th World Conference on Earthquake Engineering, 16WCEE 2017
Santiago Chile, January 9th to 13th 2017
Paper N° 2438
Registration Code: S-G1464738152

MAGNITUDE AND DISTANCE SCALING OF ENGINEERING DEMAND PARAMETERS OF MOMENT-RESISTING FRAME STRUCTURES

M. De Bortoli[(1)], F. Zareian[(2)], Y. Bozorgnia[(3)]

[(1)] *Ph.D. Candidate, University of California, Irvine, debortom@uci.edu*
[(2)] *Associate Professor, University of California, Irvine, zareian@uci.edu*
[(3)] *Professor in Residence, University of California, Berkeley, yousef@berkeley.edu*

Abstract

This paper presents a mathematical formulation that directly estimates the engineering demand parameters (EDPs) of moment-resisting frames based on structural characteristics and earthquake parameters such as magnitude, source-to-site distance and local site conditions. These equations are developed for Maximum Interstory Drift Ratio (MIDR) and Roof Drift Ratio (RDR). One set of generic elastic moment-resisting frames is used to validate the proposed formulation against the results of Response Spectrum Analysis (RSA). The results confirm that the new equations provide a conservative but accurate estimate of the structural response while simplifying the computational process.

Keywords: Probabilistic seismic hazard analysis; ground motion models; EDP hazard curve.

1. Introduction

The goal of Probabilistic Seismic Demand Analysis is the development of the EDP hazard curve λ_{EDP}, which estimates the mean annual frequency of exceeding a specified threshold of the structural response. This has traditionally been achieved using a two-step approach: First the hazard at the site is estimated based on the seismicity of the area and on the intensity measure IM chosen to represent the ground motions, obtaining the IM hazard curve λ_{IM} through Probabilistic Seismic Hazard Analysis PSHA (Cornell (1968) [1], McGuire (1995) [2]), represented by Eq. (1).

$$\lambda_{IM}(im) = \sum_{i=1}^{n} \nu_i \int_{all\ \boldsymbol{\theta}} P\left(IM > im | \boldsymbol{\theta}\right) f_i(\boldsymbol{\theta})\, \mathrm{d}\boldsymbol{\theta} \tag{1}$$

Where: $\lambda_{IM}\,(im)$ represents the mean annual frequency of exceeding the intensity measure value $IM = im$,
n is the number of potential earthquake sources at the location of interest,
ν_i is the average seismic rate of source i,
$\boldsymbol{\theta}$ represents all the ground motion parameters (magnitude, distance, etc.), and
$f_i\,(\boldsymbol{\theta})$ is the probability density function of the ground motion parameter combination for earthquake source i.

The second step is the definition of the IM-EDP relationship, which is generally developed by fitting a curve to the results of multiple nonlinear seismic analysis (see Baker (2005) [3] for a thorough review of the existing methods). Once the EDP distribution at multiple IM levels is available, it is integrated with the IM hazard curve according to Eq. (2) to obtain λ_{EDP}.

$$\lambda_{EDP}(edp) = \int_{im} P\left(EDP > edp | IM = im\right) \left| \mathrm{d}\lambda_{IM}(im) \right| \tag{2}$$

The accuracy of this approach strongly depends on the chosen IM, which is generally the pseudo-spectral acceleration at the first period of the structure $PSA(T_1)$. In his paper, Luco (2007) [4] gauges the strength of an intensity measure in terms of its efficiency and sufficiency. Several advanced intensity measures have been introduced in recent years to overcome the shortcomings of PSA (see De Biasio (2014) [5], Luco (2007) [4], Tothong (2007) [6] just to name a few), but the simplicity of calculation of $PSA(T_1)$ and its predominance in engineering practice have allowed it to remain the IM of choice to this date, including in the development of the Ground Motion Models as part of the recent NGA-West2 project, Bozorgnia (2014) [7].

This paper summarizes part of the accomplished research in a project that aims at reducing the bias introduced by the selection of an intensity measure by developing a set of Performance Prediction Equations that estimate the EDP distribution based on ground motion parameters alone. These equations can be included in any hazard calculation software to deliver the direct calculation of the EDP hazard curve according to Eq. (3).

$$\lambda_{EDP}(edp) = \sum_{i=1}^{n} \nu_i \int_{all\ \boldsymbol{\theta}} P\left(EDP > edp | \boldsymbol{\theta}\right) f_i(\boldsymbol{\theta})\, \mathrm{d}\boldsymbol{\theta} \tag{3}$$

The next section presents the formulation of the first generation of PPEs, which use the existing GMMs to estimate the EDP statistics. Section 4 presents the application of these equations to strike-slip scenarios to show the distribution of the response with several ground motion parameters and to validate the equations against conventional RSA. Additional information about the mathematical formulation and additional results will be available in an upcoming paper.

2. Formulation

As previously mentioned, the goal of this study is to develop and implement an analytical formulation that provides the EDP distribution based on ground motion parameters. The simplest way to achieve this is to use the

existing ground motion models to estimate the IM statistics, which are in turn transformed into EDP statistics using the method summarized in the following. The full mathematical derivation of the EDP statistic equations will be provided in an upcoming paper by the authors.

A simple way of generating IM-EDP relationship is to utilize response spectrum analysis - with complete quadratic combination CQC (Wilson (1981) [8]) - where the maximum SDOF responses for the first *n* modes of vibration are combined according to Eq. (4) to estimate the total response, using displacement as the EDP of interest:

$$Disp_k = \sqrt{\sum_{i=1}^{n}\sum_{j=1}^{n} Disp_{i,k}\ \alpha_{T_i,T_j}\ Disp_{j,k}} = \sqrt{\sum_{i=1}^{n}\sum_{j=1}^{n} \Gamma_i\ \Phi_{i,k}\ \frac{PSA_i}{\omega_i^{\,2}}\ \alpha_{T_i,T_j}\ \Gamma_j\ \Phi_{j,k}\ \frac{PSA_j}{\omega_j^{\,2}}} \tag{4}$$

Where: k is the story number,
i is the mode number,

$\Gamma_i = \dfrac{\int_0^1 \Phi_i(x)dx}{\int_0^1 \Phi_i^{\,2}(x)dx}$ is the modal participation factor of mode i (from Chopra [9]),

PSA_i is the pseudo-spectral acceleration at the ith mode period,
$\Phi_{i,k}$ is the ith mode shape of the structure at story k,
$\omega_i = 2\pi/T_i$ is the circular frequency of mode i,

$\alpha_{T_i,T_j} = \dfrac{8\xi^2\left(1+\frac{T_i}{T_j}\right)\left(\frac{T_i}{T_j}\right)^{\frac{3}{2}}}{\left[1-\left(\frac{T_i}{T_j}\right)^2\right]^2 + 4\xi^2\frac{T_i}{T_j}\left(1+\frac{T_i}{T_j}\right)^2}$, which is equal to 1.0 when $i = j$ (Wilson (1981) [8]),

ξ is the damping ratio, 0.05.

Eq. (4) establishes a multivariate nonlinear relationship $g(\boldsymbol{x})$ between the response variable $Disp_k$ and the pseudo-spectral acceleration at several periods, which can be approximated using Taylor series, as shown in Eq. (5):

$$Y \sim g(\tilde{\mathbf{x}}) + \sum_{i=1}^{n}(x_i - \tilde{x}_i)\frac{\partial g(\mathbf{x})}{\partial x_i}\bigg|_{\mathbf{x}=\tilde{\mathbf{x}}} + \frac{1}{2!}\sum_{i=1}^{n}\sum_{j=1}^{n}(x_i - \tilde{x}_i)(x_j - \tilde{x}_j)\frac{\partial^2 g(\mathbf{x})}{\partial x_i\,\partial x_j}\bigg|_{\mathbf{x}=\tilde{\mathbf{x}}} + \cdots \tag{5}$$

If only the linear term is used, and using the linear properties of the expectation operator, it is possible to derive formulas that provide the statistics of the response variable $Disp_k$ based on the statistics of the *PSA* vector, which are readily available from any existing GMM. It is also reasonably assumed that the distribution of the EDP be lognormal, therefore, the mean and variance of $ln\ Disp_k$ fully describe its distribution. These values are provided in Eq. (6), where $\boldsymbol{A_i}$ is a vector representing the structural properties for mode i.

$$\begin{cases} \mu_{\ln Disp,k} = \dfrac{1}{2}\ln\left(\sum_{i=1}^{3}\sum_{j=1}^{3} A_{i,k}\ A_{j,k}\ \alpha_{T_i,T_j}\ \mu_{PSA_i}\ \mu_{PSA_j}\right) = \dfrac{1}{2}\ln CQCA_k \\ \sigma^2_{\ln Disp,k} = \dfrac{1}{CQCA_k^{\,2}}\sum_{i=1}^{3}\sum_{j=1}^{3}\rho_{PSA_{ij}}\ \sigma_{PSA_i}\ \sigma_{PSA_j}\ AA_{i,k}\ AA_{j,k} \end{cases} \tag{6}$$

Where: $A_{i,k} = \frac{\Gamma_i \Phi_{i,k}}{\omega_i^2}$,

$$AA_{i,k} = A_{i,k} \sum_{t=1}^{3} A_{t,k} \mu_{PSA_t} \alpha_{T_i,T_t} ,$$

$$CQCA_k = \sum_{i=1}^{3} \sum_{j=1}^{3} A_{i,k} A_{j,k} \alpha_{T_i,T_j} \mu_{PSA_i} \mu_{PSA_j} .$$

Similar formulas can be obtained for interstory drift ratio *IDR* by using $\Delta\theta_i = (\theta_{i+1} - \theta_i)/h$ instead of θ_i, and are reported in Eq. (7).

$$\begin{cases} \mu_{\ln IDR,k} = \frac{1}{2} \ln CQCB_k \\ \sigma^2_{\ln IDR,k} = \frac{1}{CQCB_k^2} \sum_{i=1}^{3} \sum_{j=1}^{3} \rho_{PSA_{ij}} \sigma_{PSA_i} \sigma_{PSA_j} BB_{i,k} BB_{j,k} \end{cases} \quad (7)$$

Where: $B_{i,k} = \frac{\Gamma_i \Delta\Phi_{i,k}}{\omega_i^2}$,

$$BB_{i,k} = B_{i,k} \sum_{t=1}^{3} B_{t,k} \mu_{PSA_t} \alpha_{T_i,T_t} ,$$

$$CQCB_k = \sum_{i=1}^{3} \sum_{j=1}^{3} B_{i,k} B_{j,k} \alpha_{T_i,T_j} \mu_{PSA_i} \mu_{PSA_j} .$$

3. Structural models: Generic elastic moment-resisting frames

The analytical models used in this study were first developed in Drain-2DX by Zareian (2009) [10] as a set of generic elastic moment-resisting frames. Fig.1 shows the general layout of the models. These 2D frames consist of 3 bays and a variable number of stories: 4, 8, 12, and 16. Each building has a set story height of 12 ft (i.e., h = 12') and a beam span of 36 ft.

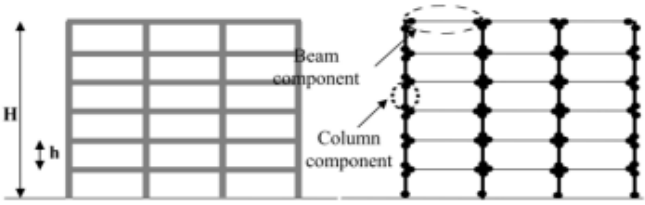

Fig. 1 – Schematic view of the generic moment-resisting frame, with the geometry on the left and the analytical model on the right (from Zareian (2009) [10])

For each number of stories, two values of the first mode period of the structure T_1 were considered: T_1 = 0.1 NS or T_1 = 0.2 NS, where NS is the number of stories. Damping was set at 5% for the first and third modes.

Three modes of stiffness distributions along the height were considered in the original report. In the "Shear" models the beam stiffness at each story varies proportionately with the story shear experienced by the building when subjected to the NEHRP lateral load pattern. This assures that the building deflected shape is linear under the same load. The "Uniform" case represents buildings with constant beam stiffness along the height, and the "Intermediate" case, as the name suggests, represents the average of the previous two at each story. Fig.2 schematically represents the variation in stiffness along the height for the three distributions. It is assumed that variation along the height of beam strength follows the stiffness distribution, based on design considerations.

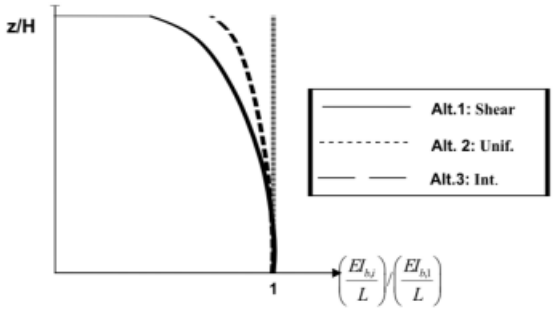

Fig. 2 – Schematic plot of the stiffness and strength variation along the height for the three distributions analyzed herein (from Zareian (2009) [10])

All beams in the same floor have equal moment of inertia and strength. The same applies to columns, and all columns in each story have the same moment of inertia as the beams in the floor above. To avoid undesirable collapse mechanisms, capacity design is implemented in the generic frames, using stronger columns than beams. All columns in the same story have equal strength as well as stiffness.

Even though the original models were designed with concentrated plasticity at the element ends, only their elastic behavior described by their modal properties is considered as part of this study. Additional information about the models can be found in the original paper, Zareian (2009) [10].

4. EDP distribution with ground motion parameters

This section presents the distribution of the structural response of the aforementioned generic buildings when subjected to several strike-slip earthquake scenarios. Only the results of the "Shear" type buildings are presented, other buildings show similar results.

The earthquake scenarios are represented by their median response spectra and their dispersions, calculated using the Campbell-Bozorgnia 2014 horizontal Ground Motion Model [11] and characteristic fault geometry considerations: Consistently with the original paper, each moment magnitude is assumed to be caused by a characteristic fault width and depth, whose values are reported in Table 1.

Table 1 – Characteristic fault geometry for strike-slip scenarios, adapted from CB14 [11]

M	Z_{BOT} [km]	W [km]	Z_{TOR} [km]	Z_{HYP} [km]
3.5	15	0.5119	7.1449	7.5626
4.5	15	1.6572	7.1449	8.2623
5.5	15	5.3653	4.2887	7.2779
6.5	15	14.1259	0.8741	8.8705
7.5	15	15	0.0	10.2267
8.0	15	15	0.0	10.2267

Five values of shear wave velocity V_{s30} are considered: 255, 360, 525, 760, and 1070 m/sec, representative of NEHRP site classes D, CD, C, BC, and B respectively, as recommended in the original paper. These strike-slip scenarios are all characterized by a 90-degree dip angle, the $Z_{2.5}$ depth was calculated from V_{s30} using Eq. (33) in CB14, and A_{1100} was calculated as the PGA value corresponding to a V_{s30} = 1100 m/sec.

The goal of this section is to validate the linearized equations developed in Section 2 by comparing the structural response calculated using these formulas with the result of response spectrum analysis RSA using the

CQC combination, introduced in Eq. (4). To provide statistical robustness to the calculations, 1,000,000 Monte Carlo simulations of $PSA(T_1)$, $PSA(T_2)$, and $PSA(T_3)$ were developed for each earthquake scenario that are consistent with the intensity measure distribution. The correlation coefficient $\rho_{lnPSA,i\ lnPSA,j}$ formulas developed in Baker (2008) [12] were used in the calculations, given the lack of updated equations.

The EDPs chosen to quantify the structural response are the Roof Drift Ratio (*RDR*) and the Maximum Interstory Drift Ratio (*MIDR*), where the height of each story is set to 12 ft. All results are presented in percentage points. Similar formulas and plots for base shear V_b were developed as part of the study, and are available upon request.

Fig.3 and Fig.4 show the distance attenuation of *MIDR* and *RDR* respectively for an 8-story structure with a first mode period T_1 of 1.6 sec located on sites with V_{S30} equal to 360 m/sec and 1070 m/sec. The median results calculated using the linearized equations are represented with a solid line while the dots are the medians of the Monte Carlo simulations. The different colors represent four values of magnitude: M = 4.5 is in red, M = 5.5 is in blue, M = 6.5 is in black, and M = 7.5 is in green. Consistently with the characteristic fault geometry assumption, the results are truncated for values of R_{RUP} lower than the depth to the top of the fault Z_{TOR}.

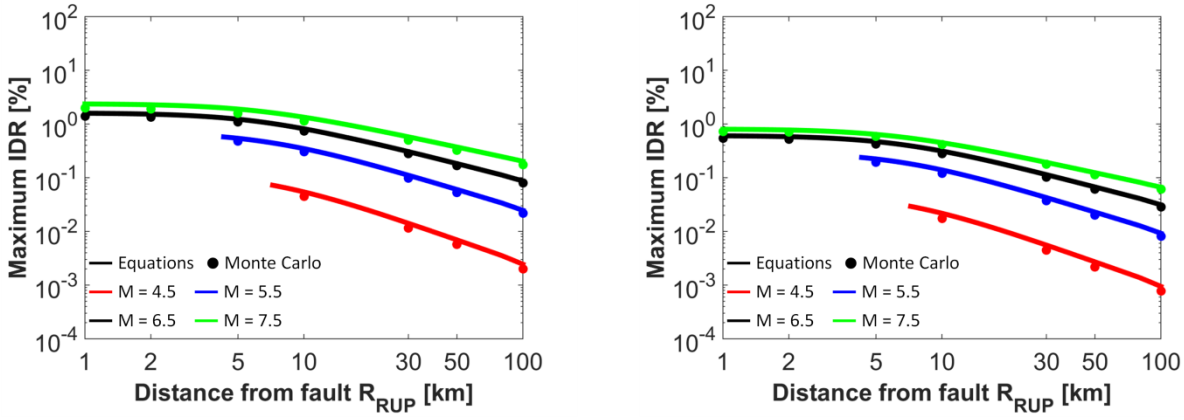

V_{S30} = 360 m/sec V_{S30} = 1070 m/sec

Fig. 3 – Distribution of median *MIDR* with distance R_{RUP} for scenarios with V_{S30} = 360 m/sec and 1070 m/sec for an 8-story building with T_1 = 1.6 sec

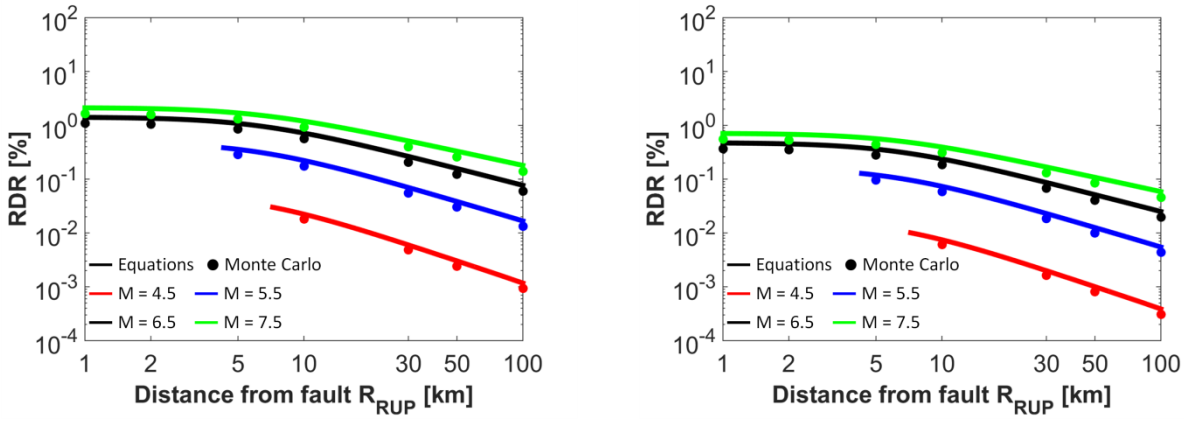

V_{S30} = 360 m/sec V_{S30} = 1070 m/sec

Fig. 4 – Distribution of median *RDR* with distance R_{RUP} for scenarios with V_{S30} = 360 m/sec and 1070 m/sec for an 8-story building with T_1 = 1.6 sec

The figures show the distance attenuation and the magnitude scaling of the results. Moreover, as expected, the structural response is generally slightly lower on stiff soil with high V_{S30} than on softer soil. The figures also show that the Monte Carlo simulations consistently fall below the solid lines, suggesting that the linearized equations offer a conservative estimate of the response. Furthermore, the small distance between the two guarantees that there is no bias when using the simplified approach.

Fig.5 offers a different perspective on the same results. The *MIDR* and *RDR* are here plotted against magnitude for four values of R_{RUP}: R_{RUP} = 5 km is in red, R_{RUP} = 10 km is in blue, R_{RUP} = 30 km is in black, and R_{RUP} = 100 km is in green. The structure is an 8-story building with a first mode period of 1.6 sec located on a site with V_{S30} = 360 m/sec. As in the previous figures, the linearized results are represented by solid lines, with interpolation of the results between magnitude values, and individual dots are used for the Monte Carlo simulations. It is easy to appreciate that the previous conclusions still apply, and the linearized equations appear to be a conservative but accurate estimate of the results.

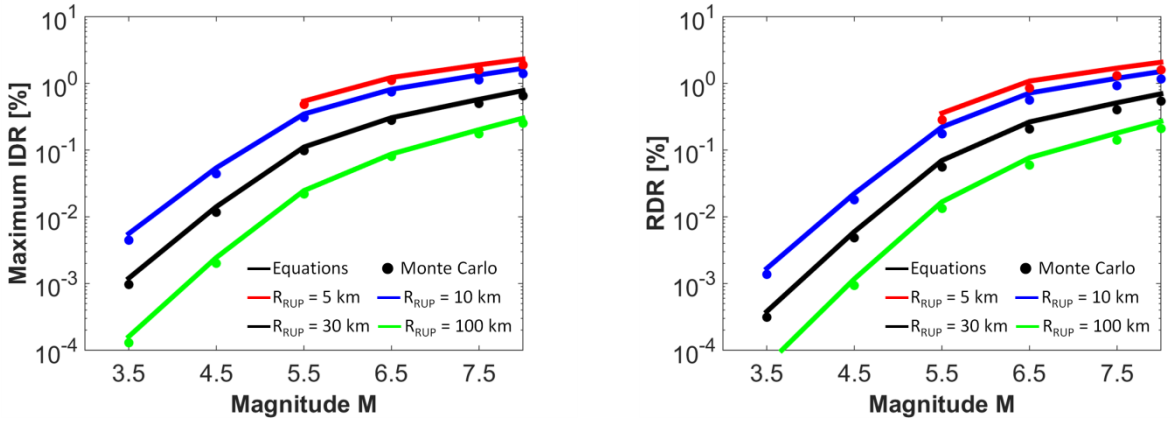

Fig. 5 – Distribution of median *MIDR* and *RDR* with magnitude for scenarios with V_{S30} = 360 m/sec for an 8-story building with T_1 = 1.6 sec

Fig.6 presents the distribution of σ_{lnMIDR} for a 12-story structure with T_1 = 1.2 sec located on soft (left) and stiff (right) soil. The results show a low dependence of the dispersion on distance and shear wave velocity, especially for more flexible structures. Magnitude appears to be the only important parameter, with slightly higher dispersion in scenarios with magnitudes in the lower range. These results are consistent with the mathematical formulation of the underlying GMM [11].

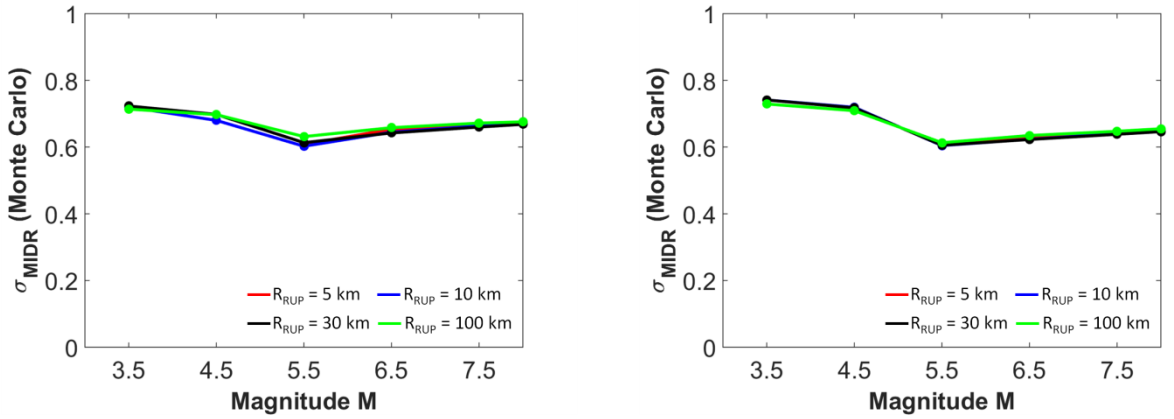

V_{S30} = 255 m/sec V_{S30} = 1070 m/sec

Fig. 6 – Distribution of σ_{lnMIDR} with magnitude for scenarios with V_{S30} = 255 m/sec and 1070 m/sec for a 12-story building with T_1 = 1.2 sec

5. Conclusions

This paper introduces a simplified mathematical formulation to determine the EDP distribution based on IM statistics. Paired with any existing ground motion model, these linearized equations can be included in any hazard software to provide a direct calculation of the EDP hazard curve. This paper reported the final equations for floor displacement $Disp_k$ and interstory drift ratio IDR_k, but the reader can find additional information on the upcoming companion paper by the same authors.

A set of generic moment-resisting frames developed by Zareian (2009) [10] was used to determine the distribution of roof drift ratio (*RDR*) and maximum interstory drift ratio (*MIDR*), using Campbell-Bozorgnia 2014 [11] as the underlying ground motion model.

The distribution of the structural response with the ground motion parameters was validated against the results of Response Spectrum Analysis (RSA) using 1,000,000 Monte Carlo simulations. The results show that the linearized equations provide a conservative and accurate estimate of the structural response.

6. Acknowledgements

This study was supported by the Pacific Earthquake Engineering Research Center (PEER). Any opinions, findings, and conclusions or recommendations expressed in this material are those of the authors and do not necessarily reflect the above organizations.

7. References

[1] Cornell CA (1968): Engineering seismic risk analysis. *Bulletin of the Seismological Society of America*, 58 (**5**), 1583-1606.

[2] McGuire RK (1995): Probabilistic seismic hazard analysis and design earthquakes: Closing the loop. *Bulletin of the Seismological Society of America*, 85 (**8**), 1275-1284.

[3] Baker JW, Cornell CA (2005): Vector-valued ground motion intensity measures for probabilistic seismic demand analysis. *Technical Report No. 150*, The John A. Blume Earthquake Engineering Center, Stanford University, Stanford, USA.

[4] Luco N, Cornell CA (2007): Structure-specific scalar intensity measures for near-source and ordinary earthquake ground motions. *Earthquake Spectra*, 23 (**2**), 357-392.

[5] De Biasio M, Grange S, Dufour F, Allain F, Petre-Lazar I (2014): A simple and efficient intensity measure to account for nonlinear structural behavior. *Earthquake Spectra*, 30 (**4**), 1403-1426.

[6] Tothong P, Luco N (2007): Probabilistic seismic demand analysis using advanced ground motion intensity measures. *Earthquake Engineering and Structural Dynamics*, 36, 1837-1860.

[7] Bozorgnia Y, Abrahamson NA, Al Atik L, Ancheta TD, Atkinson GM, Baker JW, Baltay A, Boore DM, Campbell KW, Chiou BSJ, Darragh R, Day S, Donahue J, Graves RW, Gregor N, Hanks T, Idriss IM, Kamai R, Kishida T, Kottke A, Mahin SA, Rezaeian S, Rowshandel B, Seyhan E, Shahi S, Shantz T, Silva W, Spudich P, Stewart JP, Watson-Lamprey J, Wooddell K, Youngs R (2014): NGA-West2 Research Project. *Earthquake Spectra*, 30 (**3**), 973-987.

[8] Wilson EL, Der Kiureghian A, Bayo EP (1981): A replacement for the SRSS method in seismic analysis. *Earthquake Engineering and Structural Dynamics*, 9, 187-194.

[9] Chopra AK (2012): *Dynamics of Structures: Theory and Applications to Earthquake Engineering*. Prentice Hall, 4th edition.

[10] Zareian F, Krawinkler H (2009): Simplified performance based earthquake engineering. *Technical Report No. 169*, The John A. Blume Earthquake Engineering Center, Stanford University, Stanford, USA.

[11] Campbell KW, Bozorgnia Y (2014): NGA-West2 ground motion model for the average horizontal components of PGA, PGV, and 5% damped linear acceleration response spectra. *Earthquake Spectra*, 30 (**3**), 1087-1115.

[12] Baker JW, Jayaram N (2008): Correlation of spectral acceleration values from NGA ground motion models. *Earthquake Spectra*, 24 (**1**), 299-317.